AIAA JOURNAL
Vol. 46, No. 2, February 2008

Modeling Projectile Damage in Transport Aircraft Wing Structures

Ronald L. Hinrichsen*
RHAMM Technologies, LLC, Bellbrook, Ohio 45305
Alex G. Kurtz†
Aerospace Survivability and Safety Flight, Wright–Patterson Air Force Base, Ohio 45433
John T. Wang‡ and Christine M. Belcastro
NASA Langley Research Center, Hampton, Virginia 23681
and
Jeffrey L. Parks
Illinois Institute of Technology, Chicago, Illinois 60616

DOI: 10.2514/1.26374

The objective of this paper is to quantify the damage caused by a missile impacting aircraft structures, using computational simulations. A three-step approach was taken. The first step was to investigate the effects of a simple body-on-body impact on the aircraft's wing structure. The second step was to simulate the hydrodynamic ram effects due to a high-velocity projectile impacting and traveling through a fluid-filled wing box. The third step was to add an explosive to the projectile model to investigate the combined effects of the kinetic energy of the projectile, hydrodynamic ram, and the explosive blast at various locations and incident angles. This paper presents the results of these steps in which the LS-DYNA code was used for each of the simulations. Results are presented in terms of images of damages as well as area removed.

Nomenclature

A = area
C_D = drag coefficient
k = experimental drag parameter
m = mass
V_i = initial fragment velocity at distance 0
V_f = fragment velocity at distance x
x = distance from detonation point
ρ = atmospheric density

I. Introduction

MITIGATING the effects of in-flight damage to commercial transport aircraft caused by terrorist attacks has recently become an area of great research interest. The sources of damage may include ballistic penetrators, high-explosive incendiary projectiles, and shoulder-fired surface-to-air missiles, or Man-Portable Air Defense Systems (MANPADS). Because they are inexpensive and many countries produce them, they can easily be acquired by terrorist groups. Additionally, the urban location of many airports allows terrorists to easily access areas in which aircraft are flying at very low altitudes, making the aircraft susceptible to attack.

Currently, commercial aircraft are not equipped with any countermeasures to defend against these attacks. Recent studies by government agencies and aircraft manufacturers have found that the cost of hardening the aircraft or installing countermeasures to defend against these threats is impractical because of the great expense. Therefore, it becomes necessary to determine likely damage scenarios caused by these projectiles, to enable the development of techniques to safely land the damaged aircraft using the remaining functional control systems and engines.

The objective of this paper is to quantify the damage caused by a projectile impacting aircraft structures, using computational simulations. Because there are many potential fusing selections, fragment patterns, impact locations, and incident angles for an attack, experimental testing of all possible damage scenarios is impractical. The use of validated computational models and commercial software to simulate projectile impact damage is therefore necessary.

Much of the work is of a sensitive nature, because it may potentially reveal vulnerabilities of commercial aircraft structures to the MANPADS threat. For this reason, some details were intentionally left out or obfuscated. Specific details of material properties, thicknesses, and allowables, as well as details of failure modeling, were intentionally withheld for this reason.

II. Strategy

The following steps were taken for this damage study. The first step in characterizing the damage caused by a projectile was to investigate the effects of a simple body-on-body impact on the aircraft's wing structure. In this investigation, it was assumed that there was no explosive material involved and the damage was caused by the kinetic energy of the projectile alone. The second step was to simulate the hydrodynamic ram effects due to a high-velocity projectile impacting and traveling through a fluid-filled wing box. The third step was to add an explosive to the projectile model to investigate the combined effects of the kinetic energy of the projectile, hydrodynamic ram, and the explosive blast at various locations and incident angles.

III. MANPADS Model Development

The 46th Test Wing at Wright–Patterson Air Force Base, Ohio, through its contractor RHAMM Technologies, LLC., is responsible

Presented as Paper 2128 at the 47TH AIAA/ASME/ASCE/AHS/ASC Structures, Structural Dynamics, and Materials Conference, Newport, RI, 1–4 May 2006; received 7 July 2006; revision received 27 November 2006; accepted for publication 7 December 2006.

*Senior Scientist, 332 Skyland Drive. Senior Member AIAA.
†Supervisor, Assessment Group, 2700 D Street, Building 1661, Room 005. Member AIAA.
‡Aerospace Engineer, Computational Structures and Materials Branch, Mail Stop 155. Associate Fellow AIAA.

Fig. 1 MANPADS model.

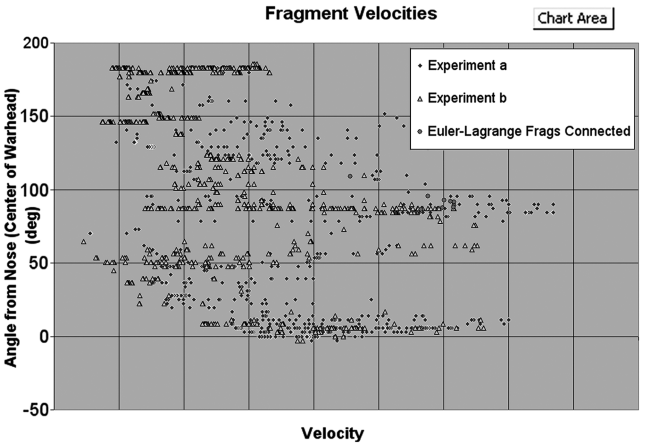

Fig. 2 Fragment velocities compared with test data.

for the body-on-body and detonation finite element analysis studies. This team has built/obtained finite element and CAD aircraft models and fabricated a MANPADS missile model [1,2]. The MANPADS missile finite element model was constructed in detail for use with the LS-DYNA [3] code and is composed of discrete sections of an actual missile (seeker, warhead, guidance and control, and rocket motor). The MANPADS missile model also contains detailed data on section properties, exterior dimensions, joint construction, joint strength, component construction, material properties, mass properties, and rocket motor case strength. Figure 1 shows a view of the model. The missile is approximately 56 in. in length, with a diameter of approximately 2.7 in.

The current version of the structural model consists of shell and solid elements. Shell elements were used to model all structural components, with the exception of the warhead, which was modeled using solids. The shell elements used are based on the Hughes–Liu formulation and are mostly quadrilaterals, although some triangles are also used. The solid elements used are all hexahedrons, and the beams are three-noded Belytschko–Schwer resultant elements. There are currently 59,821 nodes, 40,705 shell elements with 23 shell materials, and 13,400 solid elements with 228 solid materials. The fragments are modeled with 5152 rigid elements.

Materials in the structural model are varied and include glass, phenolic, aluminum, and steel. In each case, nonlinear material models are employed. The majority of these nonlinear material models are of the piecewise-linear-plasticity type. In this type of material model, density, elastic modulus, yield stress, tangent modulus, and failure strain are specified, as well as a nonlinear stress–strain curve.

Structural damage was simulated by using element erosion. In this technique, when an element reaches its failure strain, it is removed from the analysis. This provides a means of introducing voids, holes, etc., in the problem.

The warhead on the missile contains high-explosive materials that produce a significant blast pressure. The shattering of the warhead casing generates fragments as well. To obtain the correct fragment pattern and velocity distribution, a coupled fluid–structure interaction technique was chosen for this purpose. In this technique, the explosive and surrounding air were modeled as fluids in an Eulerian domain, with the air modeled using an ideal-gas equation of state, and the explosive was modeled using a Jones–Wilkins–Lee equation of state. The warhead structures, including fragments and end caps, were modeled in the Lagrangian domain. The fragment accelerations for the first several microseconds were extracted from this analysis and combined with the fragment masses (using Newton's third law) to obtain fragment-force-vs-time curves. This expensive coupled analysis was performed once and the force curves were generated. These curves were then used in a much more economical, all-Lagrangian model, of the MANPADS.

The blast characteristics of the warhead were introduced into the model using a parametric representation that was developed for the ConWep (conventional weapons effects) [4] code. ConWep is a semi-empirical code that calculates incident and reflected pressures and impulses as functions of time, given an equivalent weight of TNT and range. It was developed by the U.S. Army and integrated into LS-DYNA. The implementation was initially intended for use in engineering studies of vehicle responses due to the blast from land mines. Its use in the MANPADS application is unique to this work and some adjustments were made to match experimental data. The warhead explosive charge was mass-scaled to match peak pressure and time of arrival of the pressure pulse as a function of range [5].

Details of the implementation of ConWep are as follows: Each structural element that is to be included in the simulation for loading due to the pressure is designated by listing it in a shell or segment set. The time and location of the detonation is set at the beginning of the simulation, and when the detonation time is reached (and for each subsequent time step in the simulation), the blast pressure for each of the elements in the set is calculated and applied to the elements. Because the elements are Lagrangian in nature, they are free to move in the domain or to fail, due to their failure criteria.

Figure 2 shows a comparison of fragment velocities from the model with data obtained experimentally.

Figure 3 shows the model-generated peak pressure vs range from the warhead, compared with experimentally obtained data.

Fragment drag was accounted for by assuming a flat trajectory. Equation (1) gives the solution of the flat-trajectory problem, where V_f is the final velocity of the fragment at distance x, given an initial velocity of V_i, with mass m in air with density ρ, and the drag coefficient is given by C_D:

$$V_f = V_i \times \exp\left(-\frac{\rho C_D A}{2m} x\right) \tag{1}$$

Experimentally, many of the parameters are unknown, and so Eq. (1) is rewritten with those parameters lumped into a single parameter $k = (\rho C_D A/2m)$:

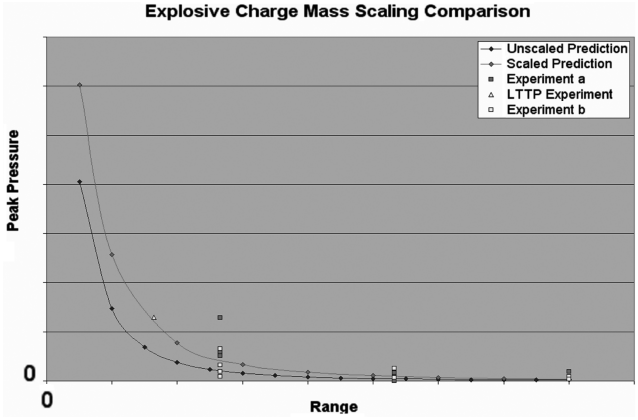

Fig. 3 Peak pressure compared with test data.

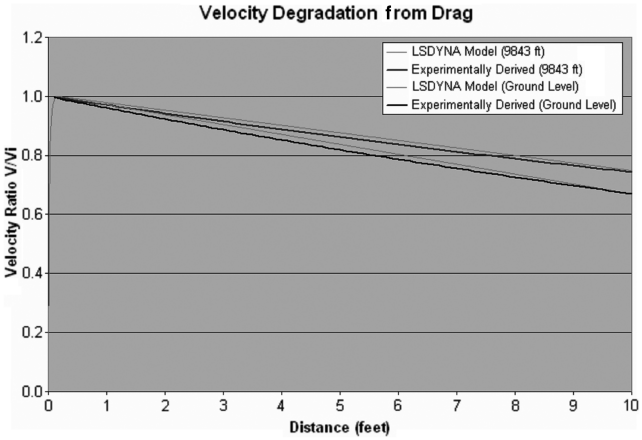

Fig. 4 Fragment velocity vs range, showing drag effects.

$$V_f = V_i \times \exp(-kx) \tag{2}$$

By measuring the velocity of individual fragments at several distances x, reasonable values for k were determined, as described in detail in [5].

Actually implementing these results into the model was done by using mass damping. Because the experiments were performed at a known altitude and density, the damping parameters are scaled according to standard atmospheric density to simulate varying altitudes at the target [5]. Figure 4 shows the quality of using this method to reproduce fragment drag at two different altitudes.

IV. Sample Target Impacts

This section shows samples of each of the three steps described in the strategy section. The first samples are of the missile impact on a target without detonation. The second samples are shown of the missile passing nearby the target and detonating as well as impacting and detonating. The last sample shown is of the missile impacting a fluid-filled wing section and introducing hydrodynamic ram. The impact velocity used for each of these samples was 1200 ft/s.

A. Step One: No Detonation

Results presented here show the body-on-body impact damages caused by a missile on a stiffened panel and a wing section. LS-DYNA was used to simulate the impact and study the size and pattern of the damage caused by the impact of the projectile at incident angles. The stiffened panel, shown in Fig. 5, was impacted by the missile with various incident angles at two different locations. One of the impact points is at the midpoint of the panel on which there is a stiffener and the other is at a midbay between two stiffeners. The stiffened panel is made of aluminum, is 30×30 in., and has 2-in. blade stiffeners at 7.5-inch intervals. The wing section shown, in Fig. 6, was impacted by the missile at a stiffened point on the lower skin. The dimensions of this wing section are as follows: the span is approximately 12 ft, the mean chord is approximately 3 ft, and the mean depth is approximately 9 in. Analysis results are discussed in the following sections. These studies and other missile impact cases will help identify the worst-case damage scenario for the prediction of the residual strength of damaged wing structures.

1. Impact by a Missile with Various Incident Angles at Midbay

The damage caused by the missile impacting at a midbay of the stiffened panel with a 0-deg incident angle is shown in Fig. 7. The missile body created a nearly circular hole in the plate approximately 3.8 in. in diameter. The impact of the fins created cracks of a total length of 4.6 in. normal to the stiffener and 5.3 in. in length in the direction of the stiffener. There was almost no deformation of either the plate or the stiffener, and the deformation was limited to only the edge of the hole.

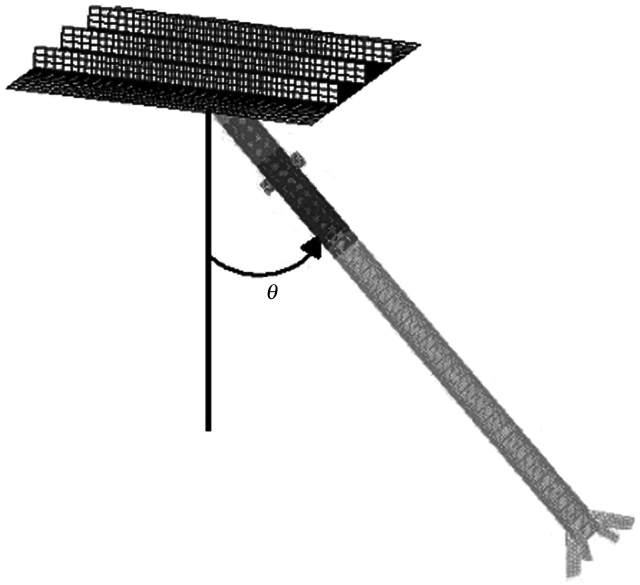

Fig. 5 Finite element model of a missile impacting on a stiffened wing panel effects.

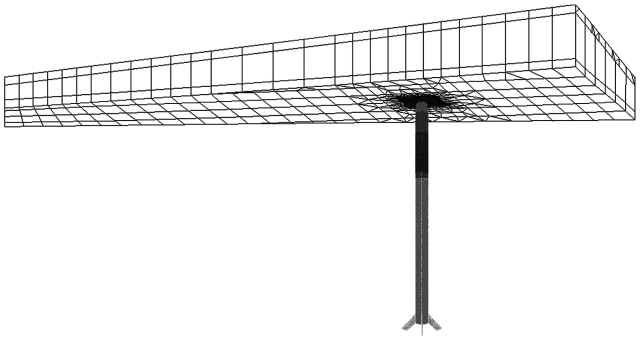

Fig. 6 Finite element model of a projectile impacting on a wing section.

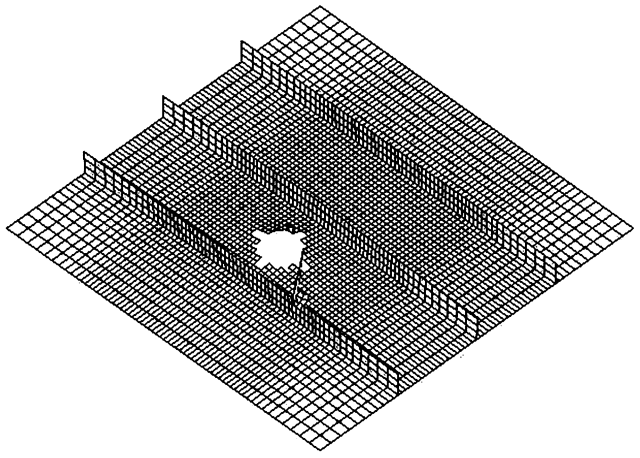

Fig. 7 Damage from 0-deg incident angle impacting at midbay.

The damage caused by the missile impacting at a midbay of the stiffened panel with a 45-deg incident angle is shown in Fig. 8. The projectile body impact created an elliptical hole 4.6 in. wide and 7.6 in. long, large enough for the fins to pass through without causing any additional damage. There was significant deformation of the plate, extending to the stiffeners on either side of the impact. This deformation caused the center stiffener to bend upward and twist away from the impact, creating a gap in the stiffener of 0.4 in.

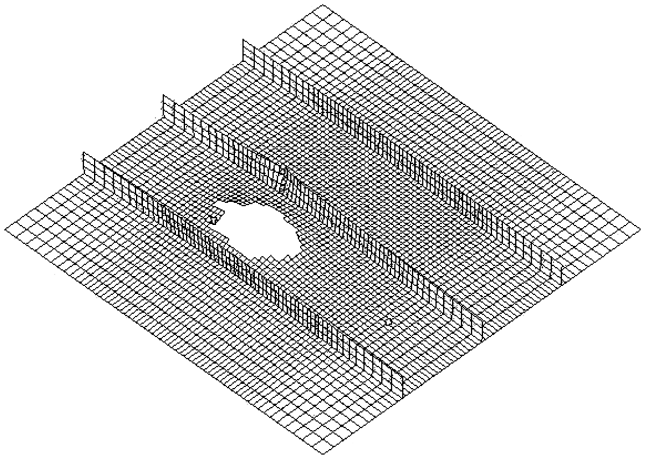

Fig. 8 Damage from 45-deg incident angle impacting at midbay.

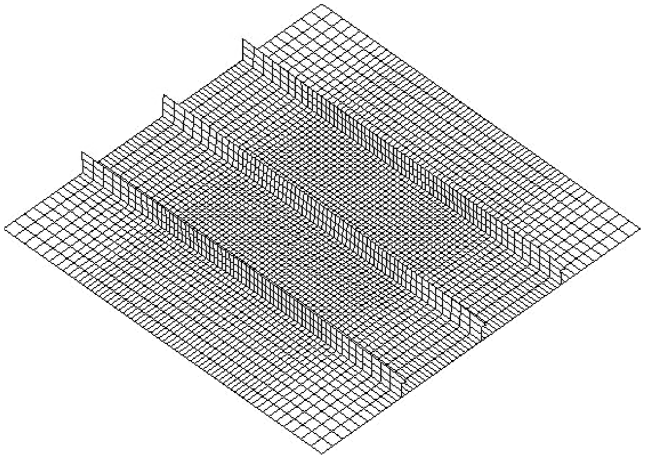

Fig. 9 Damage from 75-deg incident angle impacting at midbay.

The damage caused by the missile impacting at a midbay of the stiffened panel with a 75-deg incident angle is shown in Fig. 9. There does not appear to be any permanent damage from this impact. The section of the plate between the stiffeners is flexible enough to absorb the energy of the projectile through elastic deformation, while deflecting the projectile to move along the plate without any penetration.

2. Impact by a Missile at the Middle of the Center Stiffener

The damage caused by the missile with a 0-deg incident angle is shown in Fig. 10. The missile body created a nearly circular hole in the plate approximately 3.25 in. in diameter. The impact of the fins created cracks of a total length of 4.6 in. normal to the stiffener and 5.3 in. in length in the direction of the stiffener. The resulting gap in the stiffener was 5.1 in. in length. There was almost no deformation of either the plate or the stiffener.

The damage caused by the missile with a 45-deg incident angle is shown in Fig. 11. The impact of the missile body created a rectangular hole approximately 3.1 in. wide and 5 in. long. The impact of the fins created an additional 1.8×1.1 in. rectangular hole to the right of the main damage area and an additional 1.1×1.1 in. hole to the left of the main damage. The stiffener remained intact throughout the impact, absorbing the kinetic energy of the projectile through deformation. The upward bending of the stiffener tore cracks in the plate measuring 2.6 in. long in front of the projectile impact and 2.25 in. long behind the impact. The section of the stiffener that was impacted by the projectile was greatly damaged, with numerous cracks forming and a large amount of deformation.

The damage caused by the missile with a 75-deg incident angle is shown in Fig. 12. The missile impact split the plate, forming a 25-in.-long crack extending from 8.2 in. behind the point of impact to the edge of the plate. The width of the crack at the point of impact was 3.6 in., and the width of the crack at the edge of the plate was 8.25 in. Both the plate and the stiffener experienced a significant amount of upward bending. The stiffener broke at the constrained end at the edge of the plate 2.6 ms after the impact, when the motor portion of the missile struck the stiffener. The stiffener then began to twist, tearing a crack in the stiffener near the point of initial impact. The

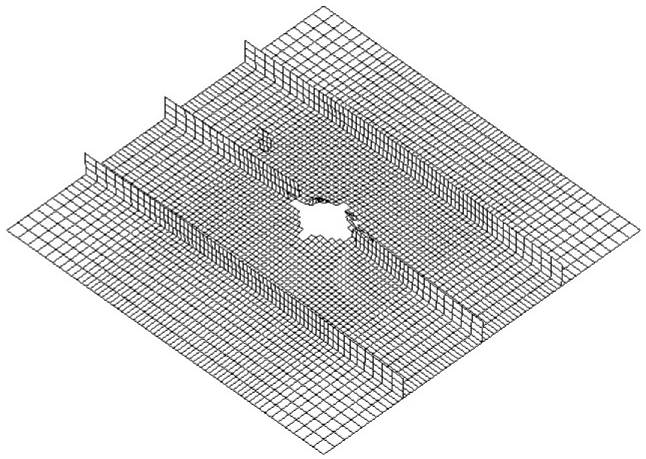

Fig. 10 Damage from 0-deg incident angle impacting at the center stiffener.

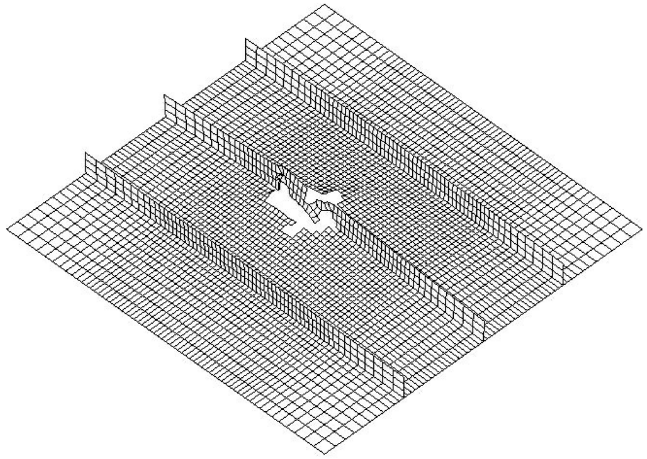

Fig. 11 Damage from 45-deg incident angle impacting at the center stiffener.

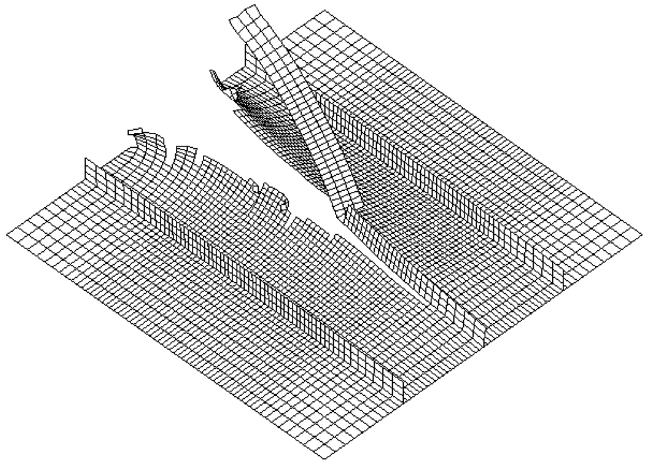

Fig. 12 Damage from 75-deg incident angle impacting at the center stiffener.

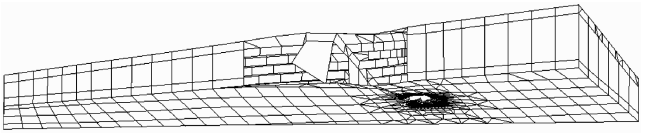

Fig. 13 Predicted damage to the wing box caused by a projectile.

15.2-in. section of the stiffener between the crack and the edge of the plate then pivoted upward, away from the projectile.

3. Projectile Damage of a Wing Section

The model used for studying the effect of a projectile impact on a representative wing box is shown in Fig. 6. Figure 13 shows the predicted damage for an impact normal to the lower skin and with the impact point lying at a stringer. The projectile penetrated through both the lower skin and the upper skin, broke a stringer on the lower and upper skins, and caused significant deformation of the structure within the impacted bay. This deformation also caused damage to the other stringers, spars, and ribs.

B. Step 2: Detonation and Fragmentation

In preparation for performing analysis of cases in which detonation and fragmentation would occur, the meshes of the target models were refined. The refinement was necessary to capture the contact of the relatively small fragments with the target. If the target elements are large relative to the fragment size, the target appears artificially stiff to the fragment and damage is not properly simulated. Following the refinement, several cases were run.

The first case presented here shows the missile passing close by a stiffened plate target at a speed of 1200 fps and not impacting the target. Three cases were run:

1) Missile fragments impact the target without blast effects.
2) Blast effects only impact the target.
3) Combined blast and fragments impact the target.

Figure 14 shows the model. Figures 15–17 show the damage due to each of the three cases. One observation that can be made from these figures is that for this very close range from threat to target, the blast effects are significant. Furthermore, one can observe the synergistic effects of the blast and fragmentation on the target.

From these quick-look simulations, one immediately sees how significant the blast and fragmentation of the warhead are when the missile is in close proximity to the target. Whereas damage due to penetration only is relatively small, the close-in detonation and fragmentation of the warhead leads to significant damage. Additional parametric studies are underway to progressively move the threat away from the target, to understand the effects of range vs damage, including the blast and fragmentation effects.

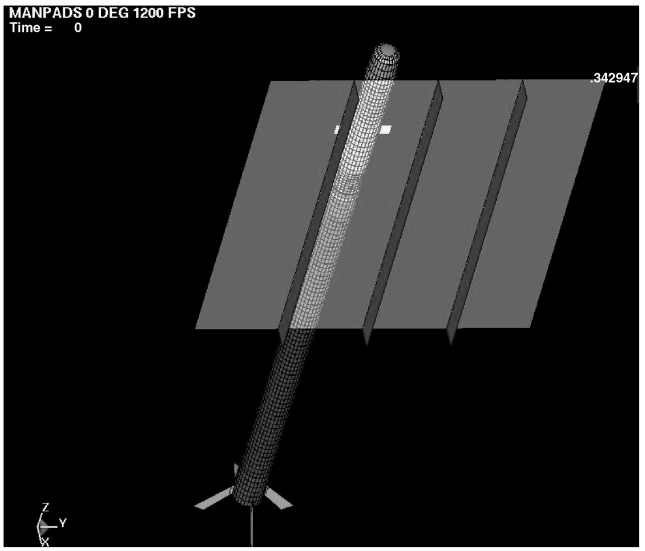

Fig. 14 MANPADS model passing close by the stiffened plate structure.

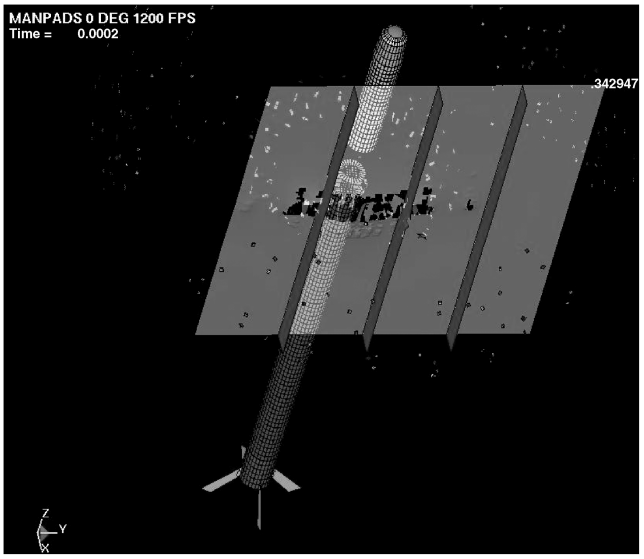

Fig. 15 Damage due to fragmentation only.

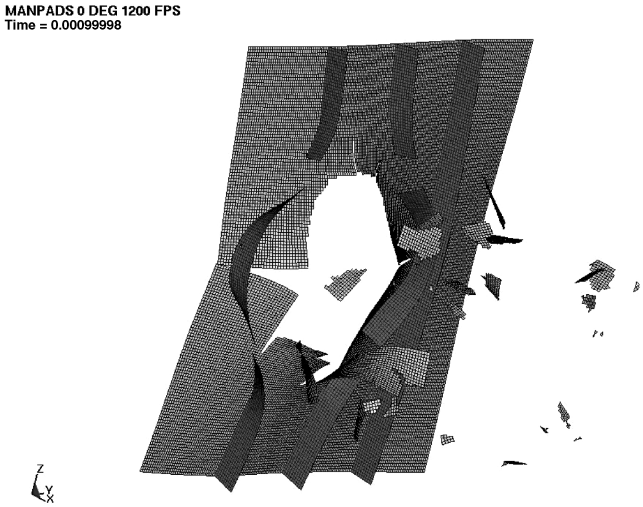

Fig. 16 Damage due to blast only.

One other item that is significant to report is that the blast is moving relative to the target. Using the *LOAD_BLAST feature of LS-DYNA assumes that the blast is located at a fixed point in space. Therefore, to simulate the moving blast, the missile is held at a fixed

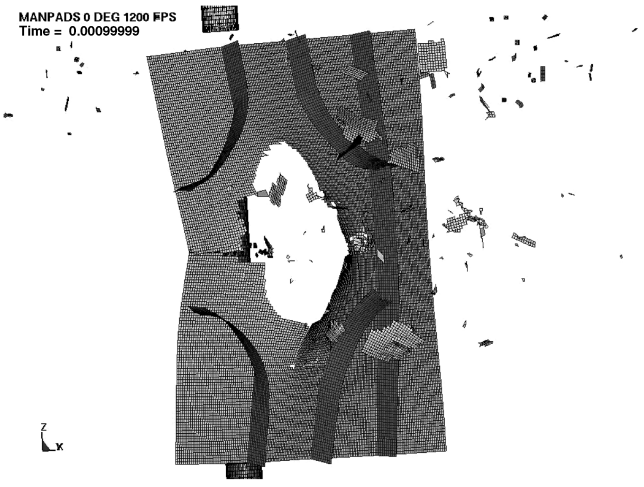

Fig. 17 Damage due to blast and fragmentation.

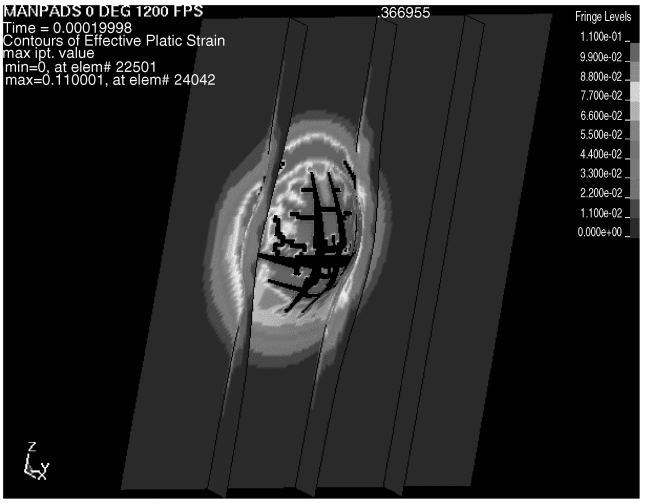

Fig. 18 Effective plastic strain showing the moving blast effects.

point and the target is moved relative to it. The resulting effects are that the blast appears to move relative to the target. Figure 18 is a snapshot in time of the plastic strain produced by the blast only. One can observe that the strain at the top of the target is significantly greater than at the bottom, indicating that the blast is moving relative to the target.

Another case of interest is presented here. This case was chosen because the corresponding nondetonating case did not show any observable damage to the structure. The case of interest is the 75-deg incident angle impacting at midbay with detonation and fragmentation. Figure 19 shows the results of this case. Comparison of Fig. 19 with Fig. 9 reinforces the observation that close-in detonation of the warhead leads to much more significant damage than penetration alone.

The last problem presented here under this step is the impact and detonation of the missile at the center of a typical wing-box structure, on which the threat hits the structure on a stiffener on the lower surface at approximately midchord. Figures 20a and 20b show the results of this encounter at 0.0044 s after impact. At this time, the threat has impacted and detonated on the lower surface, with the rocket body still traveling forward. One can observe that the rocket body is in the process of penetrating the upper surface. Figure 20a shows the damage observed from the lower side, and Fig. 20b shows the damage observed from the upper side. Note that the damage on the lower side is extensive. The upper-side damage is mainly the result of the kinetic energy imparted to the upper skin by some of the warhead fragments, as well as by the rocket body.

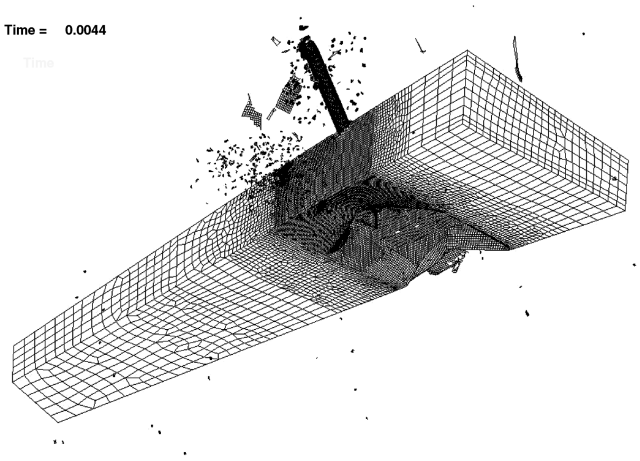

a)

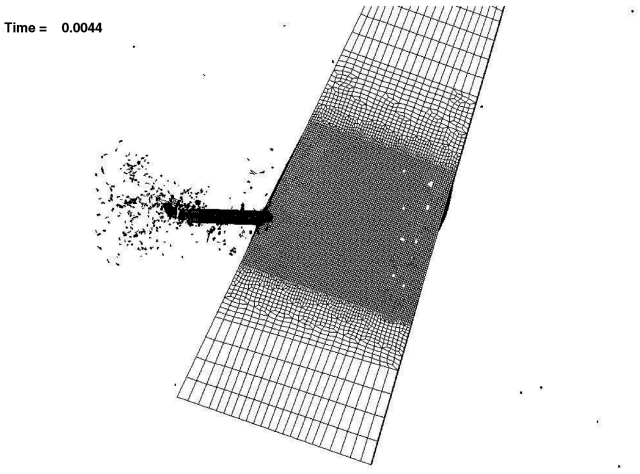

b)

Fig. 20 Damage from a 60-deg incident angle detonating on the wing box: a) bottom and b) top.

C. Step 3: Hydrodynamic Ram

One other event that is of interest is the case in which the missile does not detonate, but impacts a fuel-filled wing tank. To investigate this event, a structural model was coupled with a fluid model.

Figure 21 shows the structural model used for the hydrodynamic ram simulation. Because hydrodynamic ram is a interaction problem, a separate fluid mesh was created, as shown in Fig. 22. This model is

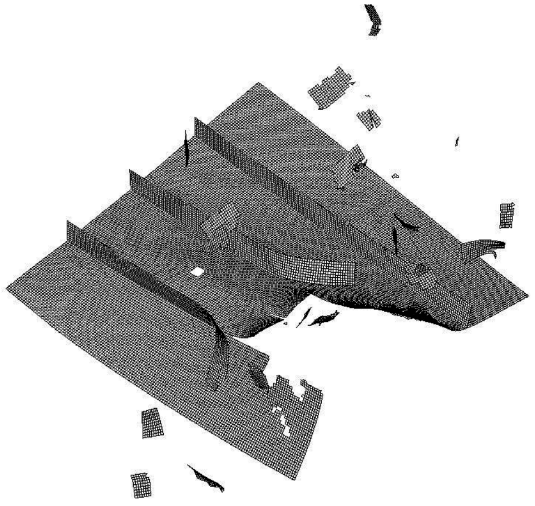

Fig. 19 Damage from 75-deg incident angle detonating at midbay.

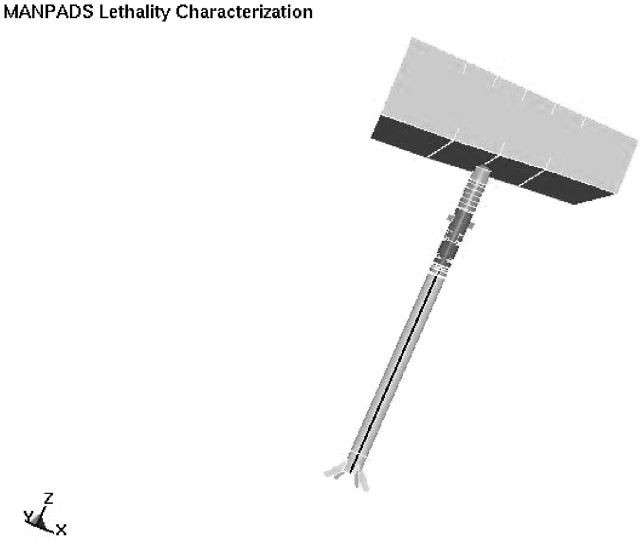

Fig. 21 MANPADS missile hydrodynamic ram model.

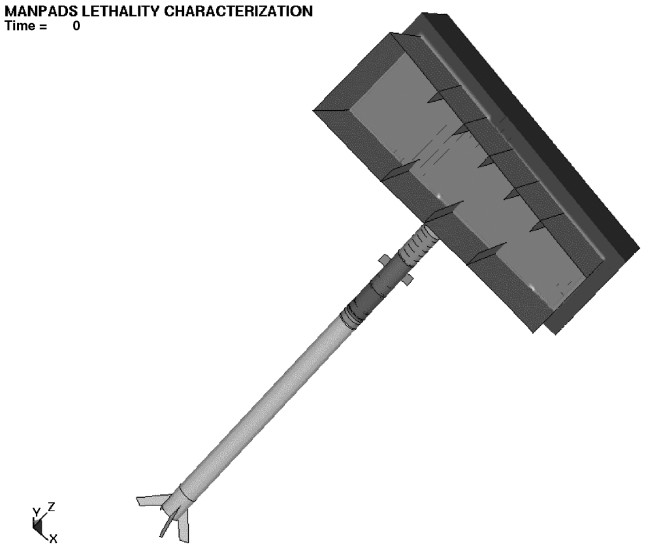

Fig. 22 MANPADS missile hydrodynamic ram model: Eulerian mesh.

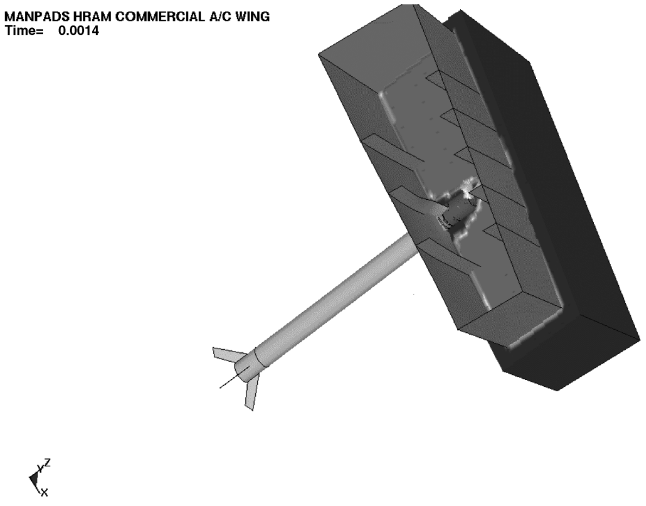

Fig. 23 MANPADS missile hydrodynamic ram model: $t = 0.0014$ s.

a multimaterial Eulerian mesh that contains air and fuel. The fuel is defined by reassigning all the Eulerian elements inside the wing structure using the *INITIAL_VOLUME_FRACTION_GEOMETRY feature in LS-DYNA. The fuel is modeled using the Gruneisen equation of state, and the surrounding air is modeled using a perfect-gas equation of state.

Figures 23–25 show the progression of the missile into the fluid-filled wing tank.

Figure 26 shows the resulting damage to the tank. Note the extensive bulging and failures at the joints of the structure. This type of damage is typical of hydrodynamic ram. This simulation leads the authors to conclude that hydrodynamic ram damage from a nondetonating missile may be significant on this class of aircraft.

V. Conclusions

This paper presents the results of a study to investigate the extent of damage that could result from impact of a Man Portable Air Defense System (MANPADS) on a typical wing structure. The study was performed analytically using an explicit finite element code, LS-DYNA, to do the simulations. The threat model was validated against experimental data and shows good agreement with the data [5].

The simulations show that if the threat impacts on a dry structure (no fuel), it will penetrate through both wing surfaces and produce

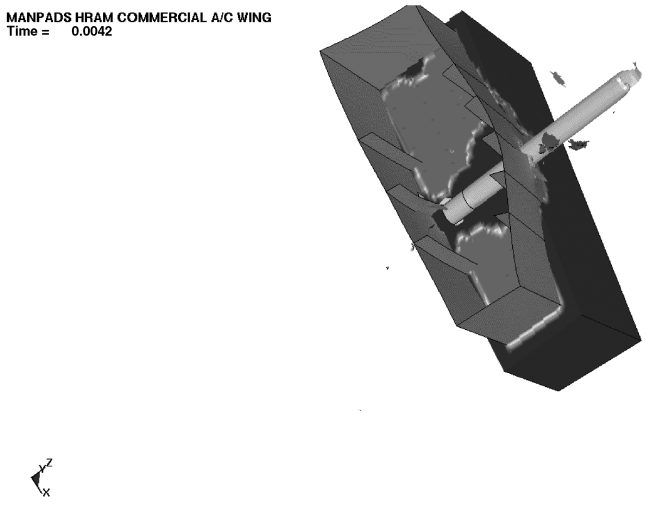

Fig. 24 MANPADS missile hydrodynamic ram model: $t = 0.0042$ s.

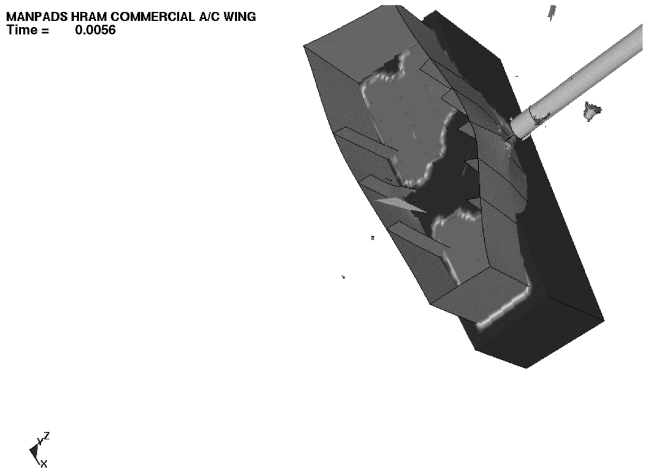

Fig. 25 MANPADS missile hydrodynamic ram model: $t = 0.0056$ s.

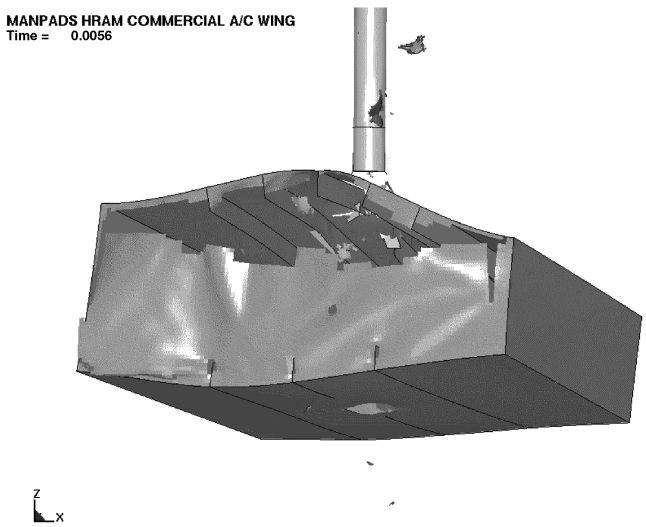

Fig. 26 MANPADS missile hydrodynamic ram model: structural damage.

hole sizes somewhat larger than the missile diameter. If the threat impacts on a wet structure (fuel tank) and does not detonate, the resulting hydrodynamic ram damage could be significant, due to the high pressure generated in the fluid. If the threat impacts and detonates on a dry structure, the damage to the impact surface and much of the internal surface could be quite extensive. The case of

detonation on a fuel-filled structure is being investigated and will be reported on in the future.

Acknowledgements

The authors wish to acknowledge that funding was provided by NASA and the Joint Aircraft Survivability Program Office (JASPO). This paper represents a large effort, involving five authors representing four organizations. The team was brought together by a common interest that emerged from discussions taking place at a review of the U.S. Air Force's Large Aircraft Survivability Initiative (LASI).

References

[1] Hinrichsen, R., and Kurtz, A., "MANPADS Analysis Methodology Developments," 43rd AIAA/ASME/ASCE/AHS SDM Conference, Denver, CO, AIAA Paper 2002-1492b, 22–25 Apr 2002.

[2] Kurtz, A., Hinrichsen, R., Moshier, M., Choules, B., and Barlow, B., "MANPADS Damage Effects Modeling, Final Report for 1 Oct. 2003–31 Mar. 2006,"Joint Aircraft Survivability Program Office Rept. V-03-08, Arlington, VA, Mar. 2006.

[3] LS-DYNA Keyword User's Manual, Ver. 970, Livermore Software Technology Corp., Livermore, CA, Apr. 2003.

[4] "Fundamentals of Protective Design of Conventional Weapons (ConWep)," U.S. Army Corps of Engineers TM-5-855-1, Washington, DC, 16 June 1988.

[5] Seymour, T. J., "Threat Characterization of Three Soviet MANPAD Warheads," U.S. Air Force Research Lab., WS-WP TR-2002-9001, Wright–Patterson AFB, OH, July 2002; also Joint Technical Coordinating Group for Aircraft Survivability, Rept. JTCG/AS-02-V-001, Arlington, VA, 2002.

T. Nicholas
Associate Editor